



# Flow-free droplet-based platform for spiral-striated polymorphic structure of periodical crystalline agglomerates

Shih-Mo Yang<sup>1</sup> · Fengjuan Chen<sup>2</sup> · Di Yin<sup>2</sup> · Hongbo Zhang<sup>2</sup> · Ruixue Yin<sup>2</sup> · Bing Zhang<sup>1</sup> · Wenjun Zhang<sup>1,2,3</sup>

Received: 27 April 2018 / Accepted: 27 September 2018 / Published online: 5 October 2018  
© Springer-Verlag GmbH Germany, part of Springer Nature 2018

## Abstract

The overarching goal of this research is to develop flow-free droplet-based platform for high-throughput and particular crystal structure directly. Crystallization plays an important role in the pharmaceutical manufacturing industry. However, the traditional on-chip approach such as the emulsion-based platform and concentric capillary tube suffers from the limitations including mixed crystal forms, broad size distribution, and incongruous crystal growth. Here, we report a study that generates single type of crystal with a particular contribution of two process parameters, namely, temperature and pH value. With our method, the droplets were formed isolated in each anchor due to surface tension, and the crystals were located as array automatically. We have successfully obtained the single  $\gamma$  form glycine crystal and spherical crystalline agglomerates array. Remarkably, the spiral-striated glycine structure of periodical crystalline agglomerates (PAs), asymmetric crystallization of droplet, crystalline shift, and shock wave expansion of crystallization energy releasing phenomenon were discovered in the first time. The distance, or named period, of inner spiral structure and their curvature radius were determined to identify PAs-2 structure. Moreover, its components and crystal forms are identified as  $\alpha$  type by X-ray diffraction analysis as well. In a word, this work provides a flow-free droplet-based platform for advancing the crystallization technology and thus extends the vision of pharmaceutical manufacturing field.

**Keywords** Flow free · Droplet-based platform · Crystallization · Glycine · Spherical crystalline agglomerates

## 1 Introduction

The crystallization process plays an important role in pharmaceutical manufacturing, and it is one of the most crucial steps in the downstream processing of the active pharmaceutical ingredients (API) (Toldy et al. 2012). Crystallization

consists of two main steps: nucleation and growth. These processes are highly dependent on the system environment parameters, such as temperature, pH value of solution, and so on (Hirata et al. 2012). Particularly, they will affect both the isolation and property of crystalline solids (Jia et al. 2007). Subsequently, the physical properties of API, including the crystal form, shape, and size, can affect the physicochemical properties of drugs such as activity, solubility, fluidity, conductivity, and so on (Rabesiaka et al. 2010). For small molecules, drugs (> 90%) are delivered to patients in a crystalline form (Variankaval and Cote 2008). The absorptivity can be enhanced if the crystals of drugs have uniform physical properties.

The crystallization process is complex to control in terms of the crystal form and shape (Toldy et al. 2012), and the process may also induce a non-ideal pesticide effect even some side effect. The starting material is also a significant factor in the crystallization process. Glycine is often used in the crystallization, for it is well known that glycine has three different polymorphs:  $\alpha$ ,  $\beta$ , and  $\gamma$  forms. The three polymorphs have their own characters. The  $\alpha$  form is

---

**Electronic supplementary material** The online version of this article (<https://doi.org/10.1007/s10404-018-2137-2>) contains supplementary material, which is available to authorized users.

---

✉ Shih-Mo Yang  
smyang@shu.edu.cn

<sup>1</sup> Biomedical Science and Technology Research Center, School of Mechatronic Engineering and Automation, Shanghai University, Shanghai 200444, China

<sup>2</sup> Complex and Intelligent Research Center, School of Mechanical and Power Engineering, East China University of Science and Technology, Shanghai, People's Republic of China

<sup>3</sup> Department of Mechanical Engineering, University of Saskatchewan, Saskatoon, SK, Canada

centrosymmetric (Marsh 1958), while the  $\beta$  and  $\gamma$  forms are non-centrosymmetric (Towler et al. 2004), and in addition, the  $\alpha$  form of glycine is thermodynamically most stable, useful, and valuable among the three forms (Titaka 1961; Park et al. 2003; Perlovitch et al. 2001; Yang et al. 2015). The  $\alpha$  form is usually obtained in an original aqueous solution (pH = 6.2), Marsh (1958), while the  $\beta$  form can be produced with high super-saturation, but it is most unstable among the three forms. Furthermore, the  $\beta$  form can readily be transformed to the  $\alpha$  or  $\gamma$  form on exposure of it to water or air (Towler et al. 2004; Srinivasan and Arumugam 2007; Allen et al. 2002; Ferrari et al. 2003; Christopher and Anna 2007).

The conventional method for glycine crystallization is stirring, which has the limitations in terms of broad size distribution, unstable crystallization environment, unpredictable crystal form, and incongruous crystal growth. The microfluidic approach is promising in overcoming the foregoing limitations (Christopher and Anna 2007; Liping; Zhu et al. 2010; Shum et al. 2008). Particularly, the emulsion-based method is very popular in the crystallization of polymorphic forms, which uses capillary microfluidics to generate monodisperse aqueous glycine-in-oil emulsion, and such a droplet is a starting point to generate crystals (Md. Badruddoza et al. 2013). Besides the importance of the state of material to start with in the crystallization process, a suitable process control is also important to result in different physical and chemical properties of crystals such as melting point and solubility (Cherukuvada and Nangia 2012). In the current literature, several studies are reported regarding the process conditions control, such as the use of “tailor-made” additives (Weissbuch et al. 1994), temperature change (Varshney et al. 2007), pH change (Lee et al. 2008). All of these methods are based on the capillary-based device, which has an inherent limitation for glycine crystallization, that is, the difficulty to adjust the parameters in polymorphic crystallization process. For example, the circumstance of a moving droplet in microfluidic channel is unstable and single  $\alpha$ - and  $\gamma$ - glycine types do not grow easily inside that (Yang et al. 2015).

The previous studies reported that the  $\alpha$  form of glycine was usually generated from an aqueous solution in the pH value ranging from 3.8 to 8.9, and the  $\gamma$  form of glycine was produced from acidic solutions (Toldy et al. 2014). The mechanism for these results was given, that is, the protonated ( $+H_3NCH_2CO_2H$ ) at low pH (< 3.8) and deprotonated ( $H_2NCH_2CO_2^-$ ) at high pH (> 8.9) inhibit the growth of the  $\alpha$  form, but the crystallization of the  $\gamma$  form has not been achieved. Lee et al. (2008) investigated the role of pH on the possibility of forming each polymorphic outcome of glycine with an evaporation-driven crystallization process from aqueous solution. They found that the pH value of solution less than 3.4 and higher than 10.10 inhibited the growth of the kinetic  $\alpha$  form, reduced the possibility of producing the

$\alpha$  form, and increased the chance of forming the  $\gamma$  form in the solution. In Yu’s study (Toldy et al. 2014), it revealed a strong pH influence on glycine crystallization during the spray drying. Compared with the frozen and freeze-dried systems (Varshney et al. 2007), the spray drying of glycine solution at low pH caused significant loss of HCl, the extent of which could be adjusted by controlling the inlet temperature of the spray dryer. Both the  $\alpha$  and  $\gamma$  forms obtained by adjusting the pH value of the solution within the range of 1.7–10.0, while the solution adjusted to higher or lower pH produced the  $\gamma$  form of glycine. This phenomenon may be attributed to the pH influence on the cyclic dimer, the elemental growth unit of the  $\alpha$  form of glycine. However, some new results different from theirs were found in our research, which will be discussed in detail later in this paper.

It is a convenient method to generate a large quantity of uniform and small volume droplets by the use of microfluidic-based platform. However, the need of a stable environment for high-quality crystallization is inevitable and the situation of a droplet inside microfluidic channel is usually moving. This work took the advantages of microfluidic fabrication to make a micro-cavities PDMS-based substrate which absorbed the trapped air inside cavity automatically and provided a stable environment for glycine crystallization in several hours or days. In another words, this nanoliter scale crystallization process overcame the limitations of stable condition than classical methods such as stirring or microfluidic device.

In this research, we report a flow-free droplet-based method for high-throughput glycine crystallization. The platform operations were aimed to be as simple as possible for a stable environment. Based on the previous technology, the operation steps such as the control of the temperature and pH value were refined and optimized. These two process parameters are hypothesized to be contributing factors to the performance of glycine crystallization, which includes polymorphic forms, size distribution, and crystal structures. Particularly, the periodical crystalline agglomerates (PAs) of glycine, crystalline shift phenomenon, radius curvature expansion, and the shock wave to surrounding disturbance via crystal growth were discovered in the first time in the literature. All of these results have provided a solid foundation for the further understanding of crystallization mechanism which is important for pharmaceutical manufacturing.

## 2 Experimental section

### 2.1 Materials

Glycine (> 99%) was purchased from Biosharp. NaOH (> 96%) was purchased from YongHua Chemical Technology. Silicone fluid (PMX-200, 10CS) was purchased from

Xiameter. Deionized water (18.3 MΩ) obtained from the purification system was used to prepare the saturated glycine solution and sodium hydroxide solution. Microscope slides (25.4 mm × 75.6 mm) were used as a crystallization platform to place the poly-dimethylsiloxane (PDMS) (Sylgard 184, Dow Corning, USA) chip. A pH hydro-tester was purchased from HM Digital.

### 2.2 Device preparation

The mold for crystallization chip was manufactured with the standard lithographic processes. The PDMS was formed from the mixture of the prepolymer A glue and B glue in the proportion of 10:1. After mixing evenly, the mixture was put in the laboratory freeze dryer (FD-1A-50, Shanghai Bilon Experiment Equipment Co., ltd.) to make the bubbles disappear. Next, the mixture was poured onto the mold and heated at 80 °C for about 180 min. Finally, the heated PDMS was peeled off from the mold, which can be used repeatedly. The platform developed here consists of 2D geometry and an array of 1024, 576, and 256 round shape indentation (anchors) was designed on the surface, at a density of 32 × 32, 24 × 24, and 16 × 16 anchors cm<sup>-2</sup> of 100 μm, 200 μm, and 300 μm diameter cavities, respectively. The processes and chip are shown in Fig. 1a–d.

The methods of high-throughput droplets in PDMS-based cavities array had the potential to number up the production results. The numbers of crystal were related on the quantity of cavities on PDMS. The cavities were molded via SU8 structure on the Si wafer. Numbering up the SU8 area is an available method to increase the crystal products. In general, the cavities array was patterned on 4 inch Si wafer. For the researchers who want to raise the production, it is suggested that increasing the number of cavity pattern properly on the whole wafer would increase the large scale crystal production upon 10<sup>5</sup> theoretically.

### 2.3 Methods

PDMS is the most widely used material for fast and easy prototyping of microfluidic devices (Kaouthar Dhouib et al. 2009). In this study, the glycine solution was expected to be trapped in the PDMS-based anchors array automatically. It is noted that the air in the anchors would block the glycine solution to get into them. To facilitate the PDMS to get trapped into the anchors space, the PDMS was put in the freeze dryer for 30 min in advance and this step enabled degassed PDMS to absorb the air from surrounding (Yang et al. 2015).

There are three different operation conditions used for examining the influence of temperature and pH value on polymorphic crystallization process.

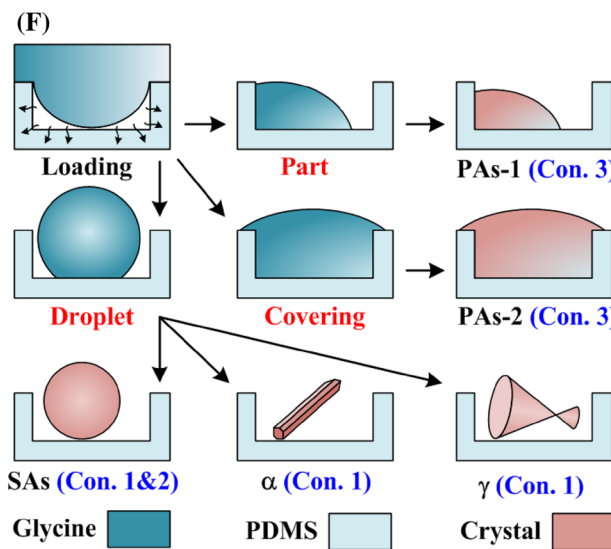
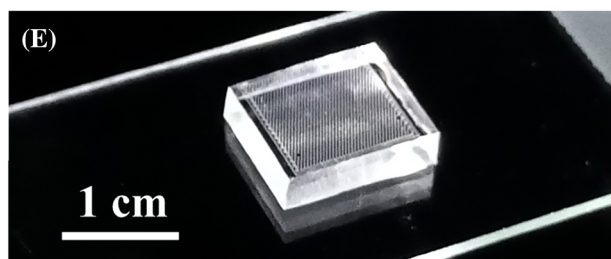
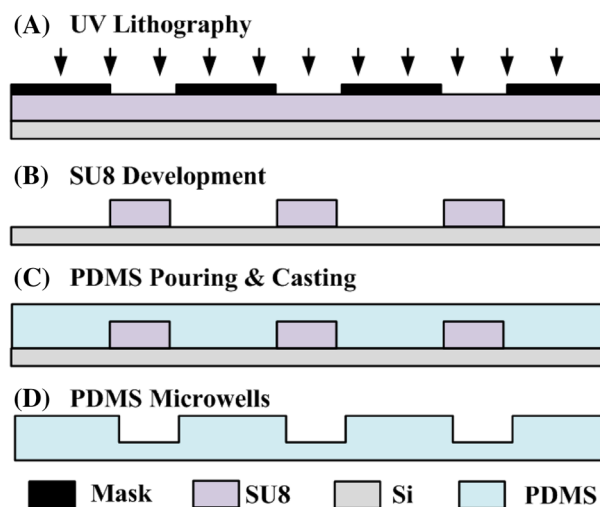


**Fig. 1** Schematic of chip fabrication. **a–d** PDMS-based chip with micro-wells array (**e**), and liquid trapping and crystallization (**f**). The glycine solution started to be driven into the anchor space because of the reduced air pressure in the bulk. Next, we took the remaining glycine solution out and covered the silicone oil. The liquid in anchor was packaged via the surface tension. When water in the glycine solution evaporated completely and a crystal formed inside anchor automatically. In Con. 1, trapped liquid formed droplet shape due to surface tension, and spherical crystalline agglomerates (SAs), α, and γ crystals were obtained. In Con. 2, most of the crystals were SAs type. In Con. 3, trapped liquid occupied part space of anchor or covered the whole microwell, and PAs-1 and PAs-2 generated in each anchor, respectively

**Condition 1 (Con. 1)** Saturated aqueous glycine (4.57 g/5 ml) solution was prepared at room temperature (25 °C) without any other solvent or additives. Then the glycine solution was covered on the surface of degassed PDMS chip. After the solution filled the space of the degassed anchors bulk (about 5 min) automatically, the remainder of the solution on the surface was removed. Next, the surface was covered with silicone oil quickly to prevent excessive evaporation of the solution. Finally, the PDMS chip was placed on a microscope slide steadily at room temperature for evaporation absolutely. The crystallization processes and crystal results were observed by a high-speed digital camera and microscope (AFNIKKDR 24-85MM/F2.8-4DIF, Nikon).

**Condition 2 (Con. 2)** Saturated aqueous glycine (4.57 g/5 ml) solution was prepared at a heating platform (FUSE 3A CMEI) without any other solvent or additives, the temperature was set at 30–80 °C. A degassed PDMS chip was placed at the heating platform for preheating (about 2–5 min). Next, the glycine solution was covered on the hot PDMS surface, and the liquid filled the anchors for a while, and then draw out the redundant solution on the surface of PDMS and cover silicone oil on the surface quickly. The PDMS was kept on the heating platform until there were some little white crystals formed in the anchors.

**Condition 3 (Con. 3)** The saturated aqueous glycine (4.57 g/5 ml) solution was prepared at room temperature (25 °C). Adjusting the pH value of the saturated solution to a range from 9.2 to 10.0 by adding appropriate sodium hydroxide (NaOH) solution. Next, the saturated solution was covered on the surface of the degassed PDMS chip to drive into the space of the anchors. After about 5 min, the remainder of the solution on the surface was drawn out and then covered with silicone fluid on the surface immediately. Then, the glycine crystallization occurred in the PDMS chip which was placed on a microscope slide at steady room temperature also was observed with the microscope.

## 2.4 Droplet packaging procedure

Figure 1f shows the schematic of crystallization formation in different operational conditions. The PDMS-based chip was degassed first and this bulk possessed the ability to absorb the air from surroundings, resulting in the reduction of air pressure in the anchor. At this time, the saturated aqueous glycine covered on the chip surface was drawn and loaded into the anchor array automatically. After the glycine solution was driven into anchor space wholly, the remaining solution was drawn out and silicone oil was taken to cover the surface of the PDMS chip immediately to prevent the solution from evaporating. The surface tension made the trapped liquid as a droplet. Silicone oil can slow down the evaporation rate and thus the solution had an enough time

for crystallization. Because the anchor contained very little liquid which volume was about nano-liter scale, the crystallization process would occur as its concentration reached saturated point. Finally, crystals would appear in the bottom of anchors after the water evaporating. There were three operational conditions for the crystallization, normal (Con. 1), temperature (Con. 2), and pH value (Con. 3). In Con. 1 and 2, the trapped liquid formed droplet shape as the surface tension balance. There were three glycine forms, SAs,  $\alpha$ ,  $\gamma$  obtained inside anchor, Con. (1) besides, the rate of SAs production was raised in Con. (2) for Con. 3, there were two kinds of trapped liquid shape, one was partly liquid occupation and the other was whole anchor covering. The results of Con. 3 were PAs-1 and PAs-2, and the details were in the following sections. The process of liquid trapped and droplet formation is demonstrated in Fig. 2.

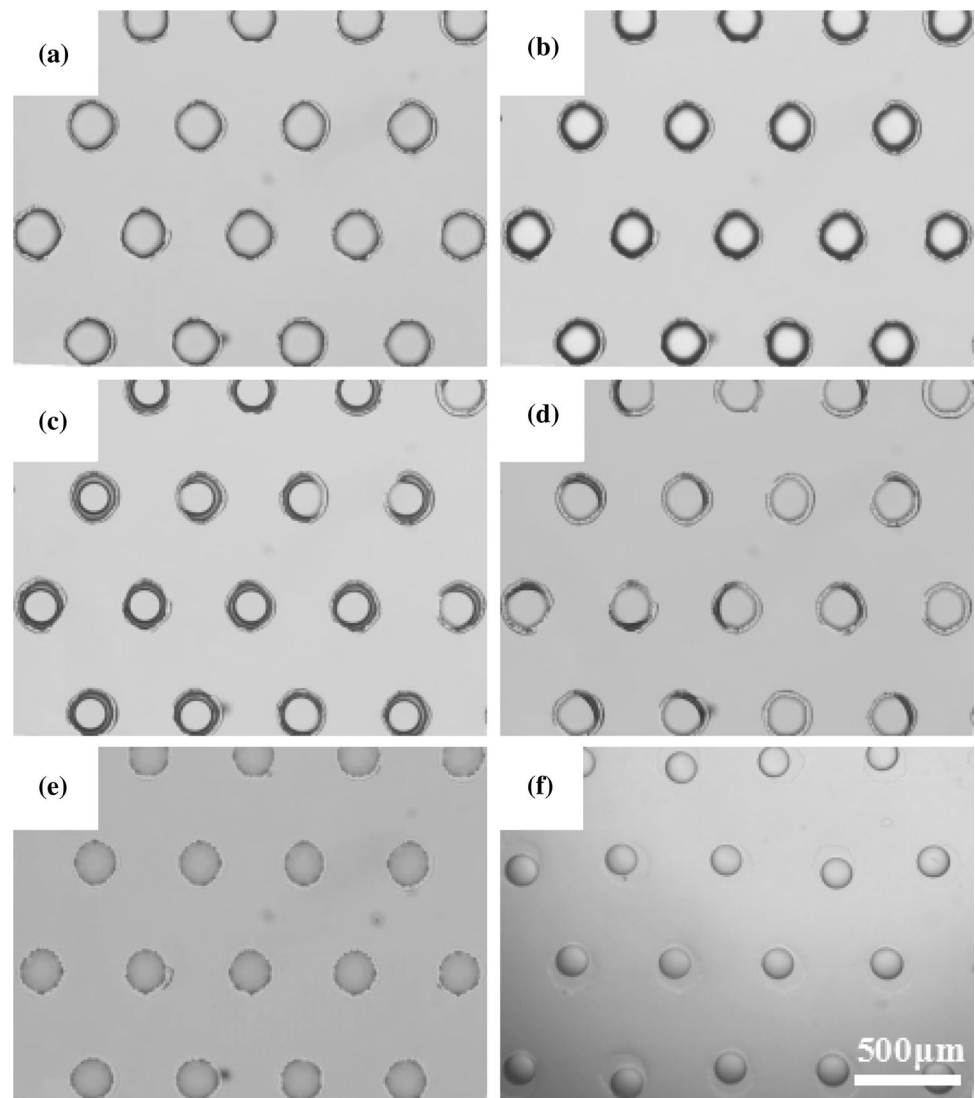
## 3 Results and discussion

### 3.1 Crystallization under Condition 1

The anchor array in the PDMS chip could separate the glycine droplets and ensure that the crystallization process would not affect each other. In addition, different crystal forms and shapes could be obtained in each anchor, but the crystal size bounded by the anchor volume was generally uniform. According to these features, the  $\alpha$ ,  $\gamma$  forms of glycine and SAs were obtained with the droplet-based method at room temperature. The glycine crystal form could be identified by its specific structure. For example, the  $\alpha$  form structure is plate, lamella, or needle-like shapes and  $\gamma$  form structure is flat at one end and pointed at the other end, like triangular pyramid structure. Just as its name implies, the structure of SAs is solid spherical shapes.

Figure 3 presents a bar chart showing the percentage of  $\alpha$ ,  $\gamma$ , and SAs within 100  $\mu\text{m}$ , 200  $\mu\text{m}$ , and 300  $\mu\text{m}$  diameters anchors under Con. 1. In the bulk aqueous solution (pH=6.2), the active  $\alpha$  form is normally obtained, and the  $\gamma$  form can also be crystallized in the neutral solution with adding some additives (Weissbuch et al. 2005), irradiation with the intense polarized laser light (Zaccaro et al. 2001), or slow solution evaporation with an evaporation-based crystallization device (He et al. 2006). Via our methods, the  $\gamma$  form could also be obtained in the micro-environment without any other additives and respective processes. More importantly, it had the biggest proportion in any size of the anchors. Due to the silicone oil covering, the solution evaporation could be slow down. That is why, a lot of  $\gamma$  forms of glycine can be produced using the method. In addition, Fig. 3b shows that the smaller size of the anchor could induce the growth of SAs.

**Fig. 2** Flow-free procedure of aqueous glycine droplet formation. The surface is patterned with a 2D array of grooves (or “anchors”) of typical depth 100  $\mu\text{m}$ . **a** Anchor array in degassed PDMS.  $t=0$  s. **b** Glycine solution was started to cover the surface of the PDMS chip.  $t=10$  s. **c, d** Trapped air was absorbed into PDMS and the glycine solution was driven into the anchor gradually.  $t=140\text{--}150$  s. About 240 s was need for the chip to absorb all air in the anchors. **e** Silicone fluid was covered on the surface of PDMS.  $t=250$  s. **f** Isolating droplets were formed as array.  $t=30$  min



Crystallization consists of nucleation and growth processes. The growth direction of crystal would be limited and SAs were more easily produced than  $\alpha$  and  $\gamma$  forms within small volume. For example, SAs' percentage in 100  $\mu\text{m}$  was about 40%. It was higher than that in 200  $\mu\text{m}$  and 300  $\mu\text{m}$ , which were about 25%. These results proposed an issue that is how to yield a high-throughput single-crystal form, e.g., SAs, in one chip. Therefore, we arranged Con. 2 to increase the rate of SAs production with temperature control.

### 3.2 Formation of SAs under Condition 2

Though SAs of glycine could be obtained at room temperature, as the previous results under Con. 1, a large batch of SAs yielded more easily at a higher temperature. As under Con. 2, the heating platform of crystallization surrounding was set at 20  $^{\circ}\text{C}$ , 30  $^{\circ}\text{C}$ , 40  $^{\circ}\text{C}$ , 50  $^{\circ}\text{C}$ , 60  $^{\circ}\text{C}$ , and 70  $^{\circ}\text{C}$ .

The results turned out that no matter what diameter of the anchor would, with the temperature being increased, the ratio of SAs increases accordingly, Fig. 4a–c. That confirmed higher temperatures did increase the water evaporating into surrounding oil environment, induce the SAs formation and accelerate the emergence of crystal nucleus. When the temperature reached 60  $^{\circ}\text{C}$  and above, almost only SAs appeared in 100  $\mu\text{m}$ , 200  $\mu\text{m}$ , and 300  $\mu\text{m}$  diameter anchors, Fig. 4c. These results shown that it needed time to generate single  $\alpha$  and  $\gamma$  forms, and their crystallization required stable environment. However, if the environment owned the tendency to enhance the crystallization rate,  $\gamma$  form was not able to produce and  $\alpha$  form grown rapidly as SAs structure. In other words,  $\alpha$  form was the main dominant of rapid glycine crystallization growth.

In the crystallization process, nucleation appeared at a random location of the droplet. Once the nucleus was formed, the crystal of glycine grew rapidly and appeared

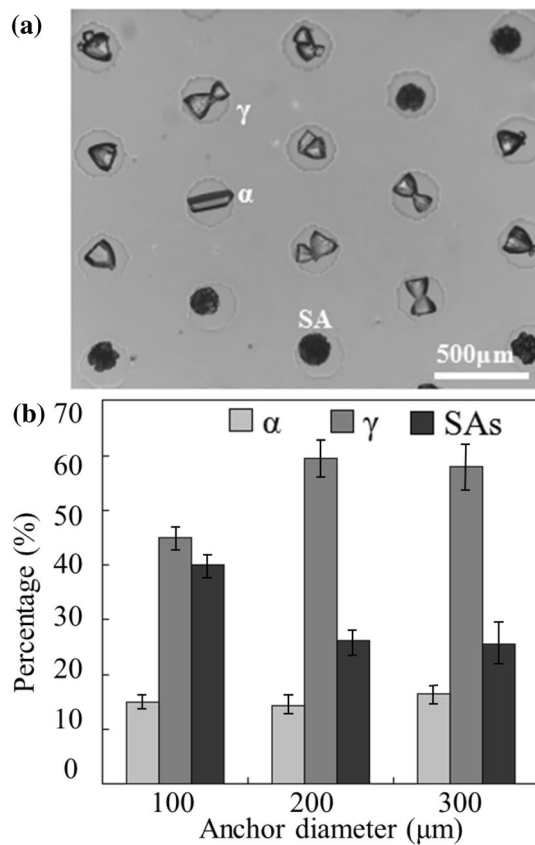


**Fig. 3** Percentage of  $\alpha$ ,  $\gamma$ , and SAs in the anchors with 100  $\mu\text{m}$ , 200  $\mu\text{m}$ , and 300  $\mu\text{m}$  diameter in under Condition 1. Whatever the anchor diameter was, the number of  $\gamma$  form glycine's appearance was the biggest. In other words, the quantity of  $\gamma$  form was more than  $\alpha$  form and SAs in the PDMS chip. Moreover, SAs almost accounted for 40% in the 100  $\mu\text{m}$  diameter anchors, and SAs had a significant increase in proportion compared with the other two sizes of the anchor, about 25%

quickly along the advancing fronts, Fig. 4d. Small cavity volume promoted the efficiency of SAs crystallization process within 1 s, and the crystal growth speed was about  $650 \mu\text{m s}^{-1}$ . Figure 4d also records the radius of curvature change when the droplet transformed into the crystal. To the best of our knowledge, this phenomenon was first time to be discovered in polymorphism crystallization. Although the shape of the droplet was like a round ball, the final crystal structure was not symmetrical shape. For analyzing this phenomenon, a crystallization model was established to mimic the process. When the crystal grew, its expansion like a shock wave and formed a wave front in all directions, Fig. 4e.  $S$  was the beginning of nucleus point and  $D$  is the droplet surface. The wave front which was round shape in all directions labelled as the blue dots line, cross section of  $W_1 \sim W_7$ .  $W_x$  was the wave front surface of crystallization expansion through  $x\Delta t$ . For example,  $W_5$  was the surface when it expanded from nucleus

point through  $5\Delta t$ . The distance and time interval between each wave front were equal and they were like concentric circles. The second image of Fig. 4d was the surface of crystallization expansion through 0.2 s. There were two reasons generating the asymmetric crystal. First, the volume was shrinking when liquid droplet transform in solid crystal. Second reason was that the time interval difference of crystallization process from one side to opposite. Shown as right image of Fig. 4e, right part of droplet was crystallized early than left part and each volume of crystal was different. We defined this phenomenon as asymmetric crystallization of droplet, ACD. If the position of nucleation was in the center and the distance of it to the surface was equivalent, the final structure was round. However, it happened quite rare. If the nucleation position was near the droplet surface and not in the center, the ACD occurred in stable environment. For investigating the change of structure, the curvature radius of the original droplet, the first half and the second half of the crystallization process were measured and written as  $R_0$ ,  $R_f$ , and  $R_s$ . The change rate of curvature radius was defined as

$$\Delta R_{f,s} = \frac{(R_f, R_s) - R_0}{R_0} \times 100\%,$$

where  $R_f$  and  $R_s$  were indicated as blue and red dots line in Fig. 4d. The curvature radius of ten images was analyzed and the results are plotted in Fig. 4f.  $R_0$ ,  $R_f$ , and  $R_s$  were about 58  $\mu\text{m}$ , 64  $\mu\text{m}$ , and 61  $\mu\text{m}$ , respectively. Therefore, the crystallization process made the radius curvature expansion in first half and second half was  $\Delta R_f = 10\%$  and  $\Delta R_s = 5\%$ . It was worth to be mentioned that this difference of crystallization process also made the solid location a little bit shift. This phenomenon was able to be observed in supplementary video 1 as well.

Because the tiny crystal was immersed in oil surrounding and its diameter was about 100  $\mu\text{m}$ , it was difficult to analyze crystal shape by our own equipment and using ImageJ software to estimate its curvature radius via 2D image is available for this work. We suggest that the following researchers are able to establish a new system with Z dimension scanning function to raise the crystal resolution and reconstruct 3D shape.

Another interesting phenomenon was that crystallization process would release energy to disturb the surrounding even generating wave propagation. Because this wave was induced from the crystal growth rapidly, like the shock wave expansion from a bomb burst, we named it as shock wave of crystallization. Yellow arrows in Fig. 4g indicated the curvature of the wave front. When the crystal grew from right to left part, this crystallization process released inner kinetic energy of action. Furthermore, the supplementary video 1 demonstrated that after whole

**Fig. 4** **a, b** SAs obtained in 100  $\mu\text{m}$  and 300  $\mu\text{m}$  diameter anchors. **c** Percentage of SAs with the anchors of 100  $\mu\text{m}$ , 200  $\mu\text{m}$ , and 300  $\mu\text{m}$  diameters under different temperatures. It was found that the higher temperature would induce the nucleation of the SAs. **d** Sequence of SAs' photographs. The crystal growth speed was about  $510 \mu\text{m s}^{-1}$ .  $R_f$  and  $R_s$  were curvature radius of first half and second half parts of solid structure, respectively. **e** Schematic of crystal growth illustrated with wave propagation model. The time interval of each wave front surface was equal, but the volume of each surface were different. **f** Curvature expansion of crystallization. The curvature radius of original droplet, the opposite points of the first half and the second half solid structure were 58  $\mu\text{m}$ , 64  $\mu\text{m}$ , and 61  $\mu\text{m}$ , respectively. **g** Shock wave expansion and propagation of surrounding disturbance due to the energy releasing of crystallization (see details in Supplementary video 1)

droplet transformed as a solid structure, this dynamic energy continued to spread in environment. The silicone oil was transparent and there were no small particles near the solid structure, and this recorded phenomenon was hypothesized via the change of refractive index. It was difficult to be observed in general microfluidics with fluid flow. Our droplet crystallization environment was stable and provided a suitable condition to record that wave propagation. This was the first report to record the shock wave of surrounding disturbance via crystal growth. Moreover, the investigation on the inner components growth as well as their energy transport, or wave mechanism, is ongoing.

### 3.3 Formation of PAs under Condition 3

It is well known that there are three glycine crystal types,  $\alpha$ ,  $\beta$ , and  $\gamma$ . Moreover, the glycine ellipsoidal crystalline agglomerates (EAs) had been firstly obtained under the rapid temperature drop condition. For expanding the manufacturing method, this work adjusted the pH value of glycine solution and found that the periodical crystalline agglomerates (PAs) could be produced in the alkaline micro-environment, whose pH value was 9.2–10.0 (under Con. 3).

These glycine crystal structures obtained under Con. 3 were very similar to EAs, and both of them had the spiral inner structure. According to the difference of crystal shapes, these results would be classed as two types. The first type, named PAs-1, was ellipsoidal agglomerates with the spiral stripe of glycine, and they were crystallized at random positions inside the anchors, Fig. 5a–c, where the dark and light stripes appeared alternately. As the light illuminating and through the crystal, the difference between light and black shadow distributions reveals the spiral inner structure. Due to the shrink of liquid drop, it also had ellipsoidal structure and possessed the side part of anchor.

Another glycine crystal type, PAs-2, was the spheroidal agglomerates with spiral stripe, and these crystals full filled the entire anchors, Fig. 5d–f. This phenomenon was hypothesized via the surface tension difference in the alkaline

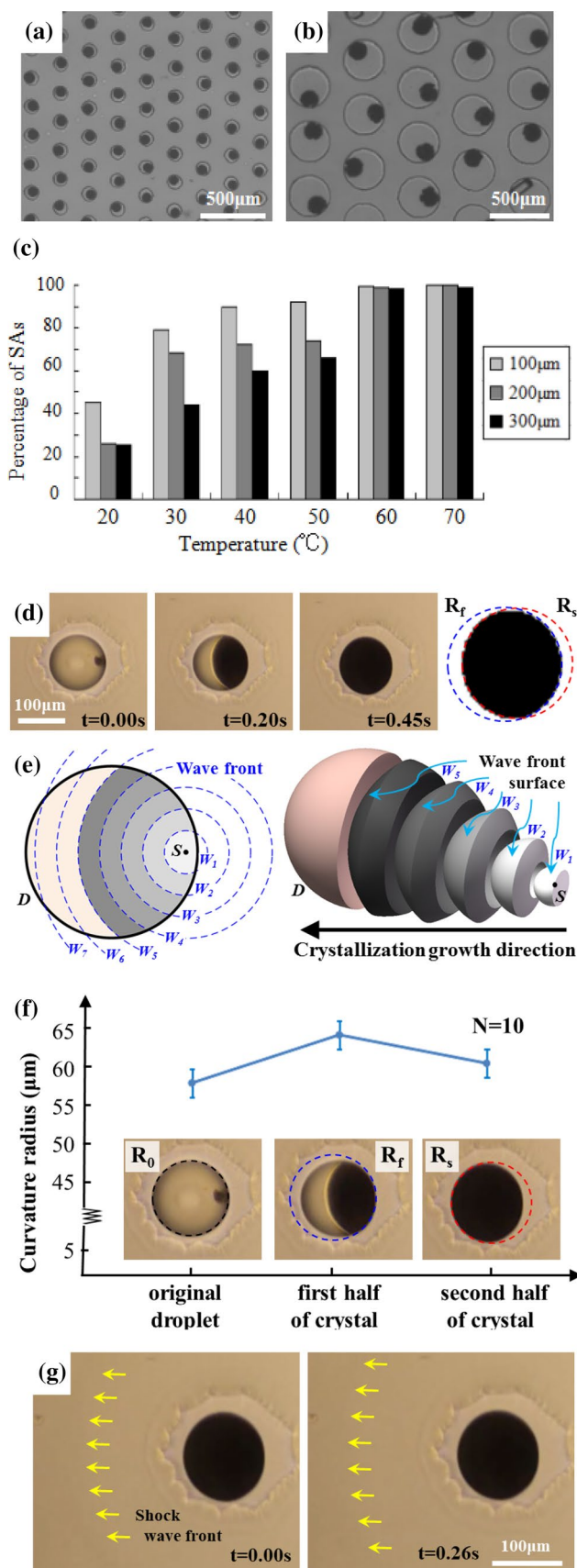
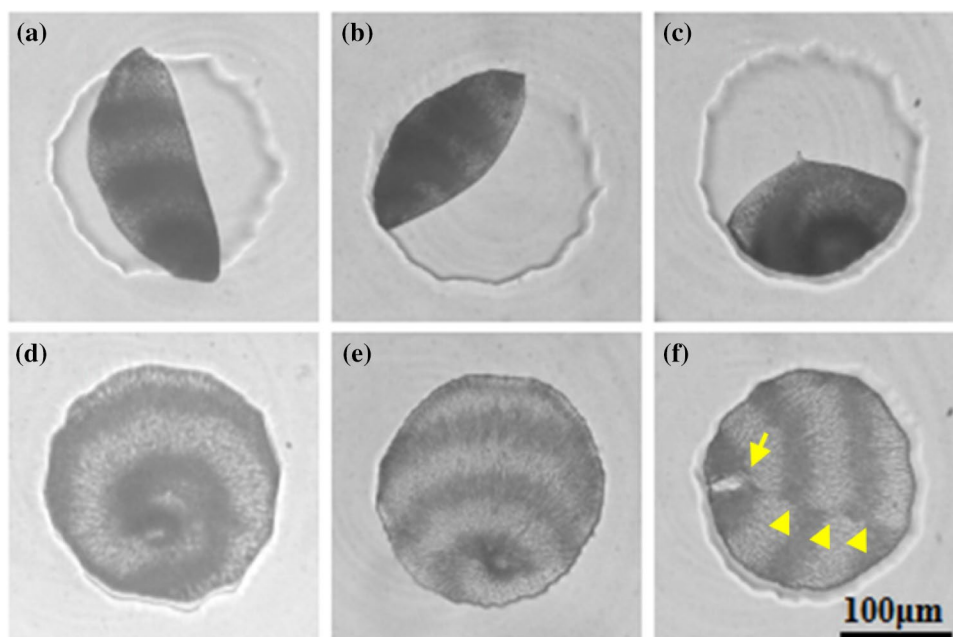


**Fig. 5** **a–c** Ellipsoidal agglomerates crystallized, PAs-1, in the anchors. **d, e** PAs-2 images observed from the tip of the spheroidal agglomerates. **f** PAs-2 spheroidal agglomerate was obtained with discrete spiral stripes. The yellow arrow and triangle indicated the interference and the boundary of crystalline shift



micro-environment. Comparing with the PAs-1, the second type had larger covering area and its spiral structure was easier to be observed.

The images at the end of the spheroidal glycine agglomerates revealed the tip of the inner spiral structure. The spheroidal agglomerates with discrete spiral stripes were recorded, Fig. 5f. There was a crystalline shift of upper and lower parts within PAs-2. The rate of this crystalline shift phenomenon was random, because its appearance needed the non-uniform crystallization expanding. Some of this action was triggered by the anchor edge of PDMS structure.

PH value of glycine solution is also another key factor of crystal growth. The micro-alkaline crystallization environment was obtained on the polymorphism of glycine. As mentioned above, the crystal shape of glycine was common and it did not generate any spiral-striated agglomerate of glycine in the macro-alkaline environment. The hypothesis for the different results may be such that in the micro-alkaline crystallization environment, the small volume limits the original crystal growth law and changes the crystal shape. However, PAs are more likely to be obtained in alkaline environment, while it did not occur in the acidic conditions. It is noted that the spiral-striated agglomerates of glycine only occurred at pH from 9.2 to 10.0. The growth theory of these periodical crystals still needs further investigation.

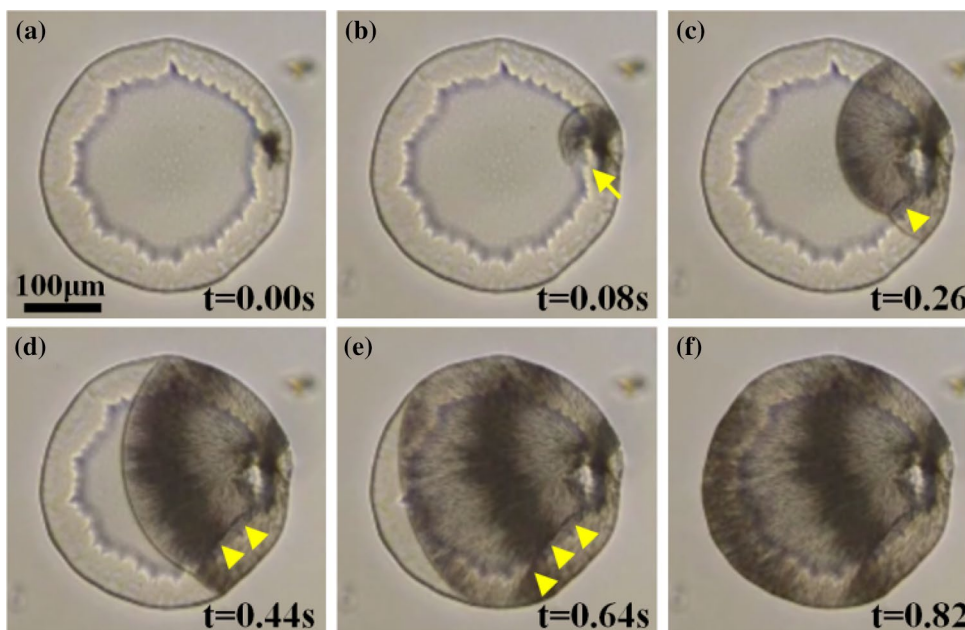
### 3.4 Dynamic PAs-2 crystallization process

The dynamic PAs-2 crystallization process was interesting and investigated by analyzing the crystallization sequence

recorded via high-speed digital camera, Fig. 6. At first, the solution concentration in the anchor was close to supersaturated via slowly water evaporation.

In most of the cases, the nucleus occurred near the edge of the cavity and then the crystallization spread from this point. In the process of crystallization diffusion, it is possible that the crystallization direction could be changed. Figure 6 records and demonstrates the appearance of crystalline shift when the crystallization expands with 15 fps frame rate. If the crystallization expanding process met the interference, crystal growth direction and velocity were sight changed, Fig. 6b. In this example, there was 100  $\mu\text{m}$  depth of the PDMS anchor and the interference was from the edge of that. Their stair difference provided a condition to generate the boundary of crystalline shift, Fig. 6c–e, indicated by yellow arrows. Because of the light refraction inside the crystal, the images looked light in some places and dark in other places, which shown the changes of crystallization structure direction and it was alternate. Therefore, there was a shift of crystal in the right down part, Fig. 6f. It turned out that the crystal growth occurred rapidly from the nucleus along advancing fronts at speed of up to  $500 \mu\text{m s}^{-1}$  during analyzing the distance and time of crystallization sequence images. The whole crystallization process only took about 1 s, but at room temperature, it needed 2–3 h for crystallization from a saturated solution of embedding in anchor to waiting for liquid reached supersaturated point. The dynamic crystallization process for the spiral structure was observed for the first time. There were five PAs-2 type crystallization processes recorded in Supplementary Video 2.

**Fig. 6** Sequence of PAs photographs. **a** Liquid was trapped over an anchor before the crystallization. The crystal nucleus was at the right location of whole aqueous. **b** When the crystallization expanded, a PDMS structure blocked a small part of the crystallization process, pointed with yellow arrow. **c** There was a boundary appeared between two different crystallization part as they expanding, pointed with yellow triangle. **d–f** As the crystallization growing whole liquid, a periodical crystal structure was formed and the yellow arrows indicated the boundary of crystalline shift. The crystal growth speed was about  $500 \mu\text{m s}^{-1}$  (Supplementary Video 2)



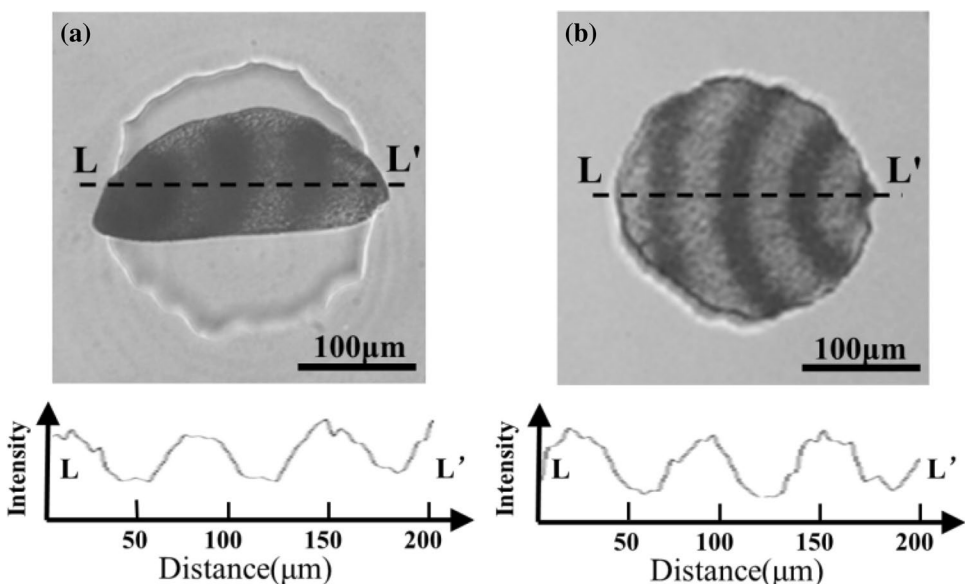
### 3.5 Periodical structure of PAs

For investigating the PAs, we applied software Image J to analysis the dark and light region of crystal images. The process of glycine crystallization diffusion would spread out from nucleus to form elliptic or concentric circular. The glycine type of PAs-1 and PAs-2, Fig. 7, was considered as the multilevel structure of concentric circles. Centered on the right drew a line along point *L* and point *L'* across the periodical crystalline part to analyze dark and gray region, and then, it obtained a data with periodic highs and lows. Mapping it as a relationship which

coordinate are intensity and distance and the distance of crystalline period was estimated to be  $50 \sim 70 \mu\text{m}$ .

In addition, the curvature radius of PAs-2 was analyzed to identify the inner glycine crystal structure. From the recorded of crystallization, supplementary video 2, it was noted that the period, or distance, of between neighboring belts was concentric circles. We chose the images which owned three dark belts for analyzing of curvature radius. The method was to select one dark belt, analyzed its edge of crystallization, and then got the center line and radius of curvature from the arc of the center line. In Fig. 8a, the three curvature radii of the dark arcs were about  $R1 = 60 \mu\text{m}$ ,  $R2 = 114 \mu\text{m}$ , and  $R3 = 167 \mu\text{m}$ . In the

**Fig. 7** **a** Image J picture of PAs-1 glycine. **b** Image J picture of PAs-2 glycine. The mapping of intensity revealed that the periodical distance of PAs was estimated to be  $50\text{--}70 \mu\text{m}$



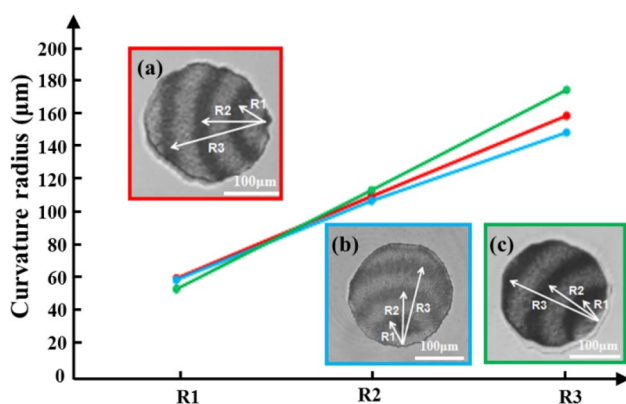


**Fig. 8** Curvature radius of inner glycine periodical structure. The distance of each radius, or the crystallization period, was about 60  $\mu\text{m}$

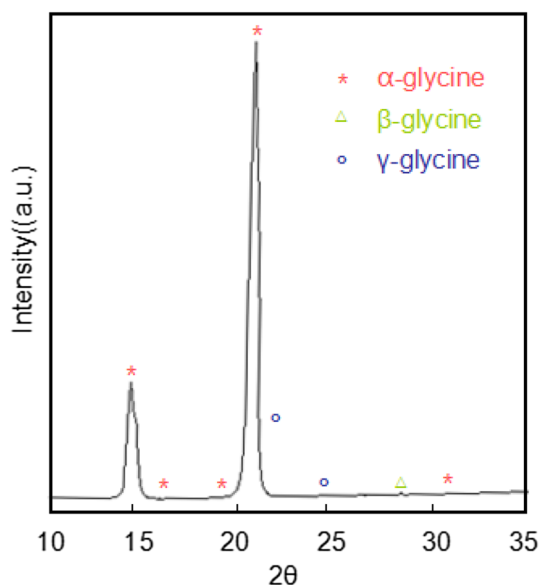


**Fig. 9** XRD characterization of the spiral-striated agglomerates obtained under Con. 3. Characteristic peak positions of all three polymorphs are indicated to confirm that the  $\alpha$  form of glycine is the dominant component

same method, in Fig. 8b,  $R_1 = 59 \mu\text{m}$ ,  $R_2 = 111 \mu\text{m}$ , and  $R_3 = 160 \mu\text{m}$ . In Fig. 8c,  $R_1 = 53 \mu\text{m}$ ,  $R_2 = 111 \mu\text{m}$ , and  $R_3 = 166 \mu\text{m}$ . These results fitted the previous estimation of concentric circles gap. The period of inner spiral structure was within the range of 50–70  $\mu\text{m}$ . Actually, supplementary video 2 shown that there were different distance of neighboring belts when the PAs-2 crystallization. For example, the crystallization period of Figs. 5d–f and 6f was different. Therefore, it was expected that this operation condition had the possible to generate larger crystallization period.

### 3.6 X-ray diffraction analysis

For understanding what kind of crystal form in PAs crystal, X-ray diffraction (XRD) was utilized to identify the crystal forms, Fig. 9, where the correspondence of peaks and crystal forms come from the literature at room temperature. For instance, the  $\alpha$  form is at  $2\theta \approx 30^\circ$ ,  $21^\circ$ , and  $15^\circ$ ,  $\beta$  form is at  $2\theta \approx 28^\circ$ ,  $24^\circ$ , and  $18^\circ$ , and  $\gamma$  form is at  $2\theta \approx 25^\circ$ ,  $22^\circ$ , and  $10^\circ$ .<sup>2</sup> In Fig. 9, the  $\alpha$  form has characteristic peaks at  $2\theta \approx 30^\circ$ ,  $21^\circ$ , and  $15^\circ$ , while the  $\beta$  and  $\gamma$  forms only appeared in minute amounts. It shown that PAs' glycine is composed of  $\alpha$  form. The measuring result is consistent with the reported studies, which researched the surface of EAs, the SEM shown EAs composed of tiny needle-like glycine crystals, and it is one of the structures of  $\alpha$  form. The SEM image of needle-like structure is shown in Fig. 8h of the previous publication.(Yang et al. 2015) In addition to that the PAs consist of thin column or needle-like shapes by microscope photographs, and above, all can prove that the spiral stripes of glycine are composed of  $\alpha$  form.

## 4 Summary and conclusions

At the field of pharmaceutical manufacturing, a large number of microfluidic operations based on dynamic droplet formation technology have become available and droplet-based platform have the feature for a range of applications. Here, we present a flow-free droplet-based platform that is unique in several important respects.

First, our flow-free method provided a stable environment for droplet and crystallization formation automatically. It was highly versatile and allowed a wide range of glycine type to be performed, such as  $\alpha$ ,  $\gamma$ , SAs, PAs-1, and PAs-2 types. Besides, it was very simple to fabricate and use, which will favor its adoption for crystallization technology and pharmaceutical manufacturing (Fig. 1). High-throughput process for single droplets and crystals revealed its potential and importance to pharmaceutical industry as well (Fig. 2).

Second, it allows a large number of time-dependent observations and crystal growth to be run in parallel.  $\alpha$ ,  $\gamma$ , and SA-type crystal can be generated on a same chip (Fig. 3). The crystallization process was able to advance by optimizing two operation parameters, temperature and pH, under three conditions. With high temperature and small volume of anchors, the rate of SAs was increased accordingly (Fig. 4c) PAs.

Third, the investigation of SAs revealed that the final glycine crystal was not symmetrical shape, although it transformed from a round ball droplet in the beginning (Fig. 4d). We built a wave propagation model inside droplet to describe this unique phenomenon, ACD. We measured its speed and the curvature radius change to calculate

its expansion rate (Fig. 4e) as well. Moreover, the energy released from the crystallization process was able to disturb the surrounding and generate a shock wave (Fig. 4g). It was the first time to demonstrate the potential of crystallization energy.

Fourth, we not generated glycine PAs, the spiral-striated glycine structure of periodical crystalline agglomerates, for the first time but determined their period of curvature radius between neighboring belts (Fig. 7). Moreover, this kind of glycine structure and crystalline shift behavior in microstructure has not been reported before (Fig. 6). These results provide evidence to the hypothesis that the direction of glycine crystallization can be cyclical changed in particular pH-value micro-environment.

Fifth, we measured the crystal growth speed of SAs and PAs-2 which range were about 500–600  $\mu\text{m s}^{-1}$ . We analyzed the periodical of spiral structure and the distance of neighboring belts was about 50–70  $\mu\text{m}$  (Fig. 8). The curvature radii of inner glycine periodical structure were measured as well. All of this information provides more detail understanding of SAs' and PAs' mechanism.

Finally, PAs was consistent with the main crystal component, tiny needle-like glycine crystals. We applied XRD to identify the component of PAs and the results confirmed that its structure was  $\alpha$  form (Fig. 9). In fast crystallization process,  $\alpha$  form was the easiest kind of crystal type to grow, gather, and expansion.

In summary, our flow-free droplet-based platform addressed a particular pharmaceutical problem and provided opportunities for variety of biological applications. For example, protein, insulin, micro- and macro- molecule synthesis and crystallizations continue to investigate by our group. The results of crystallization behavior and structure on our platform were quite different from general microfluidic methods. In the previous reports, crystallization in micro-droplet or microfluidics was usually limited by dynamic fluid flow. Therefore, the most important feature of our methods is that all the processes and operations are achieved in stable micro-environment. Furthermore, based on these results, our method is excellent candidate for application in the field of micro-reactors, lab-on-a-chip contexts, crystallization methodology, and pharmaceutical industry.

**Acknowledgements** This work was supported by Complex and Intelligent Research Center, School of Mechanical and Power Engineering, East China University of Science and Technology. The X-ray diffraction analysis was supported by BL16B1 in Shanghai Synchrotron Radiation Facility. The authors would like to thank the financial support of National Natural Science Foundation of China (21404038) and (21375166), 111 Project (D18003), the Fundamental Research Funds for the Central Universities of China (22A201514029), and Natural Science and Engineering Research Council of Canada Discovery Grant (417649).

## References

- Allen K, Davey RJ, Ferrari E, Christopher Towler A, Tiddy GJ (2002) The crystallization of glycine polymorphs from emulsions, microemulsions, and lamellar phases. *Cryst Growth Des* 2:523–527
- Cherukuvada S, Nangia A (2012) dissolving eutectic compositions of two anti-tubercular drugs. *CrystEngComm* 14:2579–2588
- Christopher GF, Anna SL (2007) Microfluidic methods for generating continuous droplet streams. *J Phys D Appl Phys* 40:319–336
- Dhouib K, Malek CK, Pflöging W (2009) Microfluidic chips for the crystallization of biomacromolecules by counter-diffusion and on-chip crystal X-ray analysis. *Lab Chip* 9:1412–1421
- Ferrari ES, Davey RJ, Cross WI, Gillon AL, Towler CS (2003) Crystallization in polymorphic systems: the solution-mediated transformation of  $\alpha$  to  $\gamma$  glycine. *Cryst Growth Des* 3:53–60
- He G, Bhamidi V, Wilson SR (2006) Direct growth of  $\gamma$ -glycine from neutral aqueous solutions by slow, evaporation-driven crystallization. *Growth Des* 6:1746–1749
- Hirata GA, Bernardo A, Miranda EA (2012) Determination of crystal growth rate for porcine insulin crystallization with  $\text{CO}_2$  as a volatile acidifying agent. *Chem Eng Process* 56:29–33
- Jia WC, Black SN, Chow PS, Tan RBH, Carpenter KJ (2007) Stable polymorphs: difficult to make and difficult to predict. *CrystEngComm* 9:128–130
- Lee IS, Kim KT, Lee AY, Myerson AS (2008) Concomitant crystallization of glycine on patterned substrates: the effect of pH on the polymorphic outcome. *Cryst Growth Des* 8:108–113
- Marsh RE (1958) A refinement of the crystal structure of glycine. *Acta Crystallogr* 11:654–663
- Md. Badruddoza AZ, Toldy AI, Hatton TA, Khan SA (2013) Functionalized silica nanoparticles as additives for polymorphic control in emulsion-based crystallization of glycine. *Cryst Growth Des* 13:2455–2461
- Park K, Evans JMB, Myerson AS (2003) Determination of solubility of polymorphs using differential scanning calorimetry. *Cryst Growth Des* 3:991–995
- Perlovitch GL, Hansen LK, Bauer-Brandl A Aspects (2001) The polymorphism of glycine. The thermochemical and structure. *J Therm Anal Calorim* 66:669–715
- Rabesiaka M, Sghaier M, Fraisse B, Porte C, Havet J-L, Dichi E (2010) Preparation of glycine polymorphs crystallized in water and physicochemical characterizations. *J Cryst Growth* 312:1860–1865
- Shum HC, Kim JW, Weitz D (2008) Microfluidic fabrication of monodisperse biocompatible and biodegradable polymersomes with controlled permeability. *J Am Chem Soc* 130:9543–9549
- Srinivasan K, Arumugam J (2007) Growth of non-linear optical  $\gamma$ -glycine single crystals and their characterization. *Opt Mater* 30:40–43
- Titaka Y (1961) The crystal structure of  $\gamma$ -glycine. *Acta Crystallogr* 14:1–10
- Toldy AI, Badruddoza AZ, Zheng L et al (2012) Spherical crystallization of glycine from monodisperse microfluidic emulsions. *Cryst Growth Des* 12:3977–3982
- Toldy AI, Zheng L, Badruddoza AZ (2014) Dynamics and morphological outcomes in thin-film spherical crystallization of glycine from microfluidic emulsions: experimental studies and modeling. *Cryst Growth Des* 14:3485–3492
- Towler CS, Davey RJ, Lancaster RW, Price CJ (2004) Impact of molecular speciation on crystal nucleation in polymorphic systems: the conundrum of  $\gamma$  glycine and molecular 'self poisoning'. *J Am Chem Soc* 126:13347–13353
- Variankaval N, Cote AS (2008) From form to function: crystallization of active pharmaceutical ingredients. *AIChE J* 54:1682–1688

- Varshney DB, Kumar S, Shalaev EY (2007) Glycine crystallization in frozen and freeze-dried systems: effect of pH and buffer concentration. *Pharm Res* 24:593–604
- Weissbuch I, Leisorowitz L, Lahav M (1994) “Tailor-Made” and charge-transfer auxiliaries for the control of the crystal polymorphism of glycine. *Adv Mater* 6:952–956
- Weissbuch I, Torbeev VY, Leisorowitz L (2005) Solvent effect on crystal polymorphism: why addition of methanol or ethanol to aqueous solutions induces the precipitation of the least stable  $\beta$  form of glycine. *Angew Chem Int Ed* 44:3226–3229
- Yang SM, Zhang D, Chen W, Chen SC (2015) A flow-free droplet-based device for high throughput polymorphic crystallization. *Lab Chip* 15:2680–2687
- Zaccaro J, Matic J, Myerson AS, Garetz BA (2001) Nonphotochemical, laser-induced nucleation of saturated aqueous glycine produces unexpected  $\gamma$ -polymorph. *Cryst Growth Des* 1:5–8
- Zhu L, Li Y, Zhang Q, Wang H, Zhu M (2010) Fabrication of monodisperse, large-sized, functional biopolymeric microspheres using a low-cost and facile microfluidic device. *Biomed Microdevices* 12:169–177

**Publisher's Note** Springer Nature remains neutral with regard to jurisdictional claims in published maps and institutional affiliations.